Industrial Chemistry: Open Access

Research Open Access

Mono or Dual-Ligand Nanoparticles: Theoretical Study

Ebtisam A Aldaais*, Shaykhah A Almaghrabi and Meernah M Alabdullah

Department of Biomedical Engineering, Imam Abdulrahman Bin Faisal University, Dammam, Saudi Arabia

***Corresponding author**: Ebtisam A Aldaais, Department of Biomedical Engineering, Imam Abdulrahman Bin Faisal University, Dammam, Saudi Arabia, Tel: + 966 555885085; E-mail: ealdaais@iau.edu.sa

Received: January 13, 2020; **Accepted:** January 28, 2020; **Published**: February 04, 2020

Abstract

Dual-ligand nanocarriers have been developed to target over-expressed receptors, such as epidermal growth factor receptors (EGFR) and folate receptors (FR), in cancer cells. The dual ligand technique has been developed to enhance nanocarrier targeting, by binding to two kinds of over-expressed receptors instead of one. This study theoretically designs the binding of dual-ligand to two types of over-expressed receptors on cancer cells. We developed molecular theory that considers van der Waals, steric, and electrostatic interactions under a decoupled Self-Consistent Field (SCF) approach. Our developed theory determines the dual-ligand-receptor binding regulations, and it can be applied for triple-ligand nanocarriers. The developed theory shows that dual-ligand nanocarriers are more effective than two mono-ligand nanocarriers combined. Manipulating some of the environmental parameters, such as salt concentration, temperature, and pH, along with the design parameters, such as polyelectrolytes pK_a, number of polymers, and their density, can improve the functionality of the therapeutic nanocarriers. Besides, the size of the targeted nanocarriers is determined in this work to an efficient binding to two or more receptors on the cancer cell.

Keywords: Nanomedicines; Drug nanocarriers; Chemotherapeutics; Tumor tissues

Introduction

A few decades ago, polymeric nanomedicines have been emerged as a promising platform to solve challenges facing cancer treatment in a selective and efficient way [1,2]. The advantages of nanomedicine technology depend on the creation of smart nanoparticles that are used as drug carriers, where they can deliver chemotherapeutics targeted to tumor tissues while screening healthy tissues [3]. The well-known examples of drug carriers are micelles [4,5], liposomes [6,7] and polymeric nanoparticles [8]. Drug nanocarriers can enhance the stability, prolong the circulation time in the bloodstream, reduce side effects, increase their accumulation in the tumor, and potentially control the release of bioactive therapeutics [1].

As the size of the nanocarriers affects their targeting and binding efficiency, various studies are conducted to identify the optimum size that can be chosen to promote their efficacy and selectivity. Some studies suggested that the nanoparticles' size should be smaller than 100 nm in diameter to be ideal for cancer therapy [9]. Other studies showed that nanoparticles and liposomes with a defined size range between 10 and 200 nm are commonly used to enhanced efficacy and reduce systemic toxicity [10-13]. Further studies showed that favored accumulation of liposomes into the tumor is reached with a specific size range between 100 and 200 nm [10]. In addition, in 2015, while Mesoporous Silica nanoparticles (MSNs) with sizes between 30 and 200 nm proved their ability to accumulate passively in tumor tissues and enhance anticancer efficacy, the cell and nucleus targeting ligand are easily conjugated to 40 nm of MSNs [14].

Drug nanocarriers are synthesized to target the over-expressed receptors in cancer cells, such as epidermal growth factor receptors (EGFR), which is involved in the proliferation and survival of the cell [15], and folate receptors (FR), which has high distribution on cancer cells, opposite to that seen on the surface of healthy cells, and presents with high affinity to improve the targeting [16-18]. Thus, most nanocarriers are synthesized with mono-ligands that can bind to EGFR or FR on malignant cells [19,20]. Several theoretical studies attempted to target one kind of receptor that is over-expressed on the tumor cells. One of them is a study of the biodegradable polymeric micelles, which are prepared to achieve FR targeted delivery of doxorubicin. The results indicated that micelles were directly transported within the cells by FR mediated endocytosis process [21]. Another study targeted EGFR on tumor cells *via* stearoyl gemcitabine nanoparticles (GemC18-NPs) to effectively control tumor growth, which significantly improved the resultant of antitumor activity [22].

In a previous study, polymeric nanoparticles with mono-ligand receptors technique were addressed through a molecular theory to acquire a distinctive ligand-receptor binding protocol. The developed theory combines three forms of molecular interactions; van der Waals, steric, and electrostatic interactions. It utilizes a decoupled mean-field approximation approach to generalize a molecular theory that determines the binding protocol [23,24]. The theory supports the understanding of ligand complex elongation by analyzing the molecular interactions in a dense none bulk system. Also, it enhances the targeting by explicitly studying several stimuli and design parameters to determine their effect on ligand complex elongation, which is vital for binding efficiency.

However, drug nanocarriers with a ligand that can bind to two kinds of over-expressed receptors have been tested to improve tumor cells targeting. The dual-ligand technique has enhanced nanocarrier targeting while sparing healthy cells [25-27]. In 2014, dual-decorated polymeric micelles with folic acid (FA) and a nuclear localization signal (NLS) for specific tumor-targeted drug delivery were tested [28]. The polymeric micelle is loaded with doxorubicin (DOX) as an anti-cancer drug, and conjugated with folic acid (FA), and a nuclear

localization signal (NLS) as ligands. The modified micelles significantly enhanced cellular uptake *via* receptor. The used nanocarriers were able to escape from the endo/lysosomes of tumor cells. Subsequently the new technique facilitated and enhanced the intracellular drug delivery, which improves the therapeutic efficiency.

In 2015, a group of researchers studied dual-ligand-modified polymer micelles [29]. The dual-ligand-modified polymer micelle is used to target both a prostate-specific membrane antigen (PSMA) and integrin αvβ3 (a tumor angiogenesis biomarker that is over-expressed in tumor neovasculature, tumor cells, and blood platelets). In 2018, constructing Salinomycin, based dual-ligand lipid-polymer nanoparticles, was studied to target EGFR for both osteosarcoma cells and osteosarcoma cancer stem cells (CSCs). This study shows that there was in anticancer activity improvement towards targeted cells compared with non-targeted or single-targeting nanoparticles. It concluded that the preparation of dual-ligand lipid-polymer nanoparticles would have promising future [30].

Our study uniquely addresses the size of the therapeutic nanoparticle to improve the targeting of malignant cells. Controlling the size of the therapeutic nanoparticle is essential to ensure the binding to the cancer cells and the screening of the healthy cells. Thus, designing the size of the therapeutic nanoparticle should depend on the density of the targeted receptor on the targeted cells. In this paper, we generated a mathematical way to calculate the optimum size of designed targeted nanoparticles. Also, the dual-ligand receptor binding is affected by the average end-to-end distance of the polymers, which is governed by the environmental conditions and the competition between the steric, van der Waals, and electrostatic forces in the system. Therefore, in this paper we study the dual-ligand-receptor binding regulation through the understanding of the molecular interactions in the system. We apply a decoupled self-consistent field (SCF) approximation to study grafted spacers and polybases-dual-ligands to a nanoparticle in a cubic lattice system with a coordination number of six [23].

Details about the thermodynamic properties of the system under study are discussed in the model section. The generalized theory is discussed through the free energy of the system in the theoretical approach section. Relevant results and comparison with our mono-ligand model is discussed in the results section. Finally, we discuss a brief conclusion on the ligand-receptor binding properties.

Nanoparticle's size

The size of the therapeutic nanoparticle usually depends on the polymers that the nanoparticle is made of or the polymers that are attached to its surface; their length, density, solubility, pH and temperature sensitivity. Specifying the size of the therapeutic nanoparticle is significant for optimum targeting and drug delivery release. The designed size of the therapeutic nanoparticle should depend on both; the density of the targeted receptors and the properties of its polymers. Although the targeted receptors occur on both healthy and cancerous cells, the density of the targeted receptors differs significantly between healthy and malignant cells. For example, the density of epidermal growth factor receptors (EGFR) in malignant cells can be 100 times higher than in normal cells [31]. Implementing the density of the targeted receptors on the design of the nanoparticle should improve the targeting and screen the healthy cells. Therefore, there should be precise therapeutic nanoparticles for a specific treatment. The density of EGFRs, as an example, which is targeted in most cancer treatments [19,31-33], differs on different types of cancerous cells Table 1 [34,35].

Cell Type	EGFR Density	Area contains or more EGFR	Nanoparticle's radius for < R >= 10
A431 [35]	1.272/2000 nm^2	4000 nm^2	45 nm
Hela [35]	1.35/5000 nm^2	10^4 nm^2	120 nm
A549 [35]	1.42/10^4 nm^2	2 × 10^4 nm^2	495 nm
MCF-7 [36]	1/2200 nm^2	4400 nm^2	50 nm

Table 1: Nanoparticle's size according to EGFR density.

Designing a large nanoparticle that could bind to several EGFRs on a healthy cell forms several bonds that could stabilize the nanoparticle on the healthy cell against the blood stream, which is illustrated in Figure 1a. Moreover, Figure 1b illustrates the binding possibility of a small nanoparticle to an individual EGFR on a healthy cell. One should aim to design an optimum therapeutic nanoparticle with a precise size that allows it to bind to a minimum of two over-expressed receptors on the cancerous cell Figure 1c. Moderating the nanoparticle size, leads to an increase of the binding forces that results in an increased stability of the nanoparticle on the cancerous cell surface against the blood stream. Thus, the choice of the size of the therapeutic nanoparticle is critical for effective treatment [23].

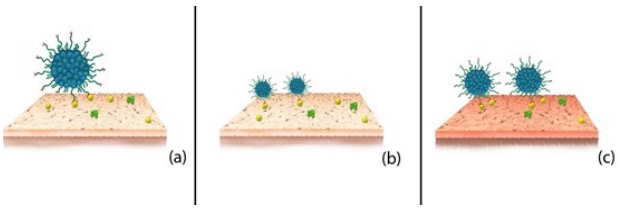

Figure 1: An illustration shows the dependency between the nanoparticle size and the receptor density on healthy and malignant cells.

Figure 1a represents a large nanoparticle that binds to a healthy cell with low density of EGFR. Figure 1b shows the ability of small nanoparticles to bind to EGFR on a healthy cell. Finally, Figure 1c illustrates the optimum binding between two ideal-sized nanoparticles and EGFRs on a cancerous cell, where the size of the nanoparticles depends on the EGFR density.

To design the optimum size of the nanoparticle we evaluate the size of the interaction surface area between the nanoparticle and the cancerous cell. The area of that surface should be equal to double the area that holds a minimum of one of the targeted receptors. Doubling the size of the interaction area allows a minimum of two ligands on the nanoparticle to bind to two receptors on the malignant cell. hus, if the density of our targeted receptors is d nm $^{-2}$, then the interaction surface area, A_{int}, is given as $A_{int}=2/d$ nm^2. he next step is to find the radius of the nanoparticle that has an interaction surface area equal to A_{int}. To do so, we look into a cross-section view of a therapeutic nanoparticle that is shown in Figure 2 and the triangle abc. Considering the length

of the side of the computed interaction area ($S=\sqrt{A_{\text{int}}}$) and theaverage length of the polymers $\langle R \rangle$ one can compute the nanoparticle's radius (r) by applying Pythagoras theorem.

$$r = \frac{1}{8}\frac{A_{\text{int}}}{\langle R \rangle} - \frac{1}{2}\langle R \rangle$$

Table 1 shows the optimum nanoparticles' radius for different cancerous cells.

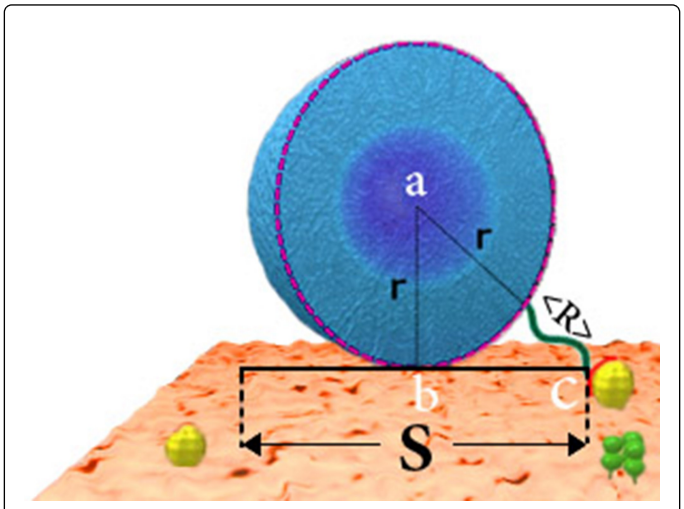

Figure 2: An illustration represents a circular cross section shape of a nanoparticle and the length of the interaction area between that nanoparticle and the targeted cell.

Model

In this study, we model the micellar surface with two different kinds of polymers (ligand complexes and spacers), where each has N_m number of monomers and a total density of σ_p. We study the interaction between the ligand complexes (basic polyelectrolytes that are attached to two ligands) on the micellar surface and two different receptors on the cell surface. The cell surface has two over-expressed targeted receptors (R_1, R_2), with densities of σ_{R1}, and σ_{R2} respectively. The other kind of polymer is spacer polymers, which are used to increase the solubility and improve the biocompatibility of the therapeutic micelle.

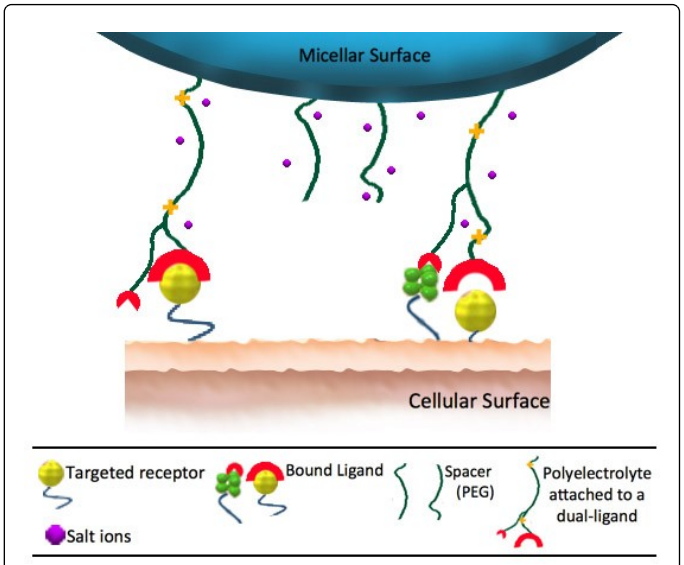

Figure 3: A model of the side to side interaction between the nanoparticle's surface and the targeted cellular surface.

The cellular surface has a specific density of receptors, while the nanoparticle's surface has two different kinds of polymers; spacers and ligand complexes. The spacers are thermoresponsive polymers, while complex ligands are positively charged polybases that are attached to ligands to target specific receptors on the cell.

The expression, "ligand complex" will be used to represent a polyelectrolyte that is attached to a dual-ligand. The polyelectrolytes in the system are polybases, which are polyelectrolytes that have basic groups. The basic groups (B) on the ligand complex are able to protonate in the biological aqueous environment into positively charged ions through the chemical reaction ($B + H^+ \xrightarrow{K_d} BH^+$), where Kd is the dissociation constant for the chemical interaction. As the ligand complexes stretch, they expose their ligands to the two different receptors (R_1, R_2) on the cell surface causing an increase in the binding probability. The ligand-receptor (LR1, LR2) binding interactions can be described by the following relations: $L + R_1 \xrightarrow{K_{LR_1}} LR_1$ and $L + R_2 \xrightarrow{K_{LR_2}} LR_2$

Where K_{LR1} and K_{LR2} are the association constants for these chemical reactions. The two association constants are defined as follows (Equation 1):

$$K_{LR_1} = \frac{[LR_1]}{[L][R_1]} = C\exp\left(-\beta(\mu^0{}_{LR_1} - \mu^0{}_L - \mu^0{}_{R_1})\right) \quad (1)$$

$$K_{LR_2} = \frac{[LR_2]}{[L][R_2]} = C\exp\left(-\beta(\mu^0{}_{LR_2} - \mu^0{}_L - \mu^0{}_{R_2})\right)$$

The fraction of ligands in the system is given by $X_L = \frac{N_L}{N_L + N_S}$ where N_L and N_S refer to the number of ligands and spacers respectively. The fraction of bound dual-ligands to receptors $R_1$and R_2

is given by the following relations:$f_{LR_1} = \frac{[LR_1]}{[LR_1]+[LR_2]+[L]}$ and $f_{LR_2} = \frac{[LR_2]}{[LR_1]+[LR_2]+[L]}$

where $[LR_1]$, $[LR_2]$ and $[L]$ are the concentrations of bound ligands to receptors (R_1, R_2), and free ligands respectively. The density of all molecules in the system is given as follows:

Spacers: $\sigma_s = \sigma_p(1 - X_L)$

Free ligands: $\sigma_L = X_L\sigma_p\left(1 - f_{LR_1} - f_{LR_2}\right)$

Bound ligands, or bound receptors: $\sigma_{LR_1} + \sigma_{LR_2} = \sigma_p X_L\left(f_{LR_1} + f_{LR_2}\right)$

Unbound receptors: $\left(\sigma_{R_1} - \sigma_p X_L f_{LR_1}\right) + \left(\sigma_{R_2} - \sigma_p X_L f_{LR_2}\right)$

The system is modeled in a cubic lattice structure with a coordination number of six. Each polymer segment or receptor molecule occupies a single cubic lattice site. Polymer conformational structures (α) are built randomly using self-avoiding random walk (SAW) with the Rosenbluths weighting technique to improve the statistics [36]. The remaining cubic sites are filled randomly with water and salt ion molecules. All molecules in the system are subject to different kinds of forces, such as steric, van der Waals and electrostatic forces.

An incompressibility constraint is applied to maintain the repulsive steric interactions between all molecules in the system. The mathematical representation of the constraint is as follows (Equation 2):

$$\langle\ \emptyset_s(z)\rangle + \langle \emptyset_L\ (z)\rangle + \langle \emptyset_{LR_1}(z)\rangle + \langle \emptyset_{LR_2}\ (z)\ \rangle + \emptyset_\omega\ (z) + \emptyset_{H^+}\ (z) + \emptyset_{OH^-}\ (z) + \emptyset_+\ (z) + \emptyset_-\ (z) + \emptyset_R = 1 \quad (2)$$

where, $\langle\ \emptyset_{ii}\ (z)\ \rangle$ is the average volume fraction of polymer ii, and $\emptyset_{jj}\ (z)$ is the volume fraction of specie jj.Notice that the system studies four different polymers: spacers (s), free ligand-complexes (L), and ligand-complexes that are bound to receptors (LR1 and LR2). Thus, $\emptyset_P\ (z)$ is the average volume fraction of polymer p, and $\emptyset_x\ (z)$ is the volume fraction of specie x.

The van der Waals interactions are accounted for in each configuration (α) through the intra-molecular interactions ($E_{\text{intra}}\ (\alpha)$) between segments of one polymer, and the inter-molecular interactions ($E_{\text{inter}}\ (\alpha)$) between polymer segments from different polymers. We use our decoupled MF approach to improve the accuracy in calculating the inter-molecular interactions [4]. The values of these two short-ranged molecular-attractive interactions, ($\varepsilon_{\text{intra}}$ and $\varepsilon_{\text{inter}}$), depend on the choice of polymers in the system and their interaction with the solvent. Moreover, the electrostatic interactions between two charged molecules in the system are influenced by several variables, such as: the surface charge coverage on the cell (σ_q), the biological salt concentration (C_{salt}), and the local pH. We study the effect of those variables on the extension of the ligand complexes. Different electrostatic interactions cause different configurations and accordingly, different intra and inter-molecular interactions. The model demonstrates the complexity of the chemical equilibrium and the physical interactions between all molecules in the system on the two different ligand-receptor bindings probabilities (P_{LR1} and P_{LR2}).

Theoretical approach

We discretize the space between the micellar surface and the cell surface into discrete layers in the *XY* plane with thickness *dz*. The system is assumed to be homogeneous in planes parallel to the cell surface and the micelle surface (*XY*), and inhomogeneous in the norm direction (*Z*). The molecular interactions are described in the system through the SCF approximation. The Helmholtz free energy per unit area for the system has the following form:

(F=F_{pol} + F_{elc} + F_{chem} + F_{if} + F_{mix})

The theory describes the system by calculating the most probable configuration of spacers, free ligand complexes and bound ligand complexes. Minimizing the free energy and introducing Lagrange multipliers π(z) allows the calculation of the three different probabilities that describe the system. The probability of having a spacer (P_s) at specific configuration (α), and the probability of having a free ligand complex or a bound ligand complex (P_{ii}) at specific configuration (α), where $ii \equiv \{L, LR_1, LR_2\}$, are given by the following relations:

$$P_s(\alpha) = \frac{W_R}{q_s}\exp\left(-\beta\left[E_{intra}\ (\alpha) + E_{inter}\ (\alpha)\right] - \beta \int \pi(z)\, v_s(\alpha, z)\, dz\right) \quad (3)$$

$$P_{ii}(\alpha) = \frac{W_R}{q_{ii}}\exp\left(-\beta\left[E_{intra}\ (\alpha) + E_{inter}\ (\alpha)\right] - \beta \int \pi(z)\, v_{ii}(\alpha, z)\, dz - \beta \int q_p n_{ii}(\alpha, z)\psi(z)\, dz - \int n_{ii}(\alpha, z)\ \ln\left(1 - f_{H^+}(z)\right) dz\right) \quad (4)$$

where q is the partition function of the corresponding polymer, and it satisfies the condition that $\sum_\alpha P(\alpha) = 0$. The Rosenbluth weighting function (WR) is used to improve the statistics of all possible polymer configurational structures [36]. The first two terms in all probabilities account for the intra and inter-molecular interactions between polymer segments, where $\beta = \frac{1}{K_B T}$ is the inverse thermodynamic temperature. The inter-molecular interactions are calculated with our decoupled MF approach [37]. In the third term of

both Equations 3 and 4, $\upsilon_s(\alpha,z)$ and $\upsilon_{ii}(\alpha,z)$ are the volume fractions of a spacer, free ligand, bound ligand to receptor R1, or bound ligand to receptor R2 that occupies layer at configuration (α). The extra two terms in equation 4, account for the electrostatic interactions as this equation describes the probability of the free and bound ligand complexes that are made of polybases. In the fourth term of equation 4, qp is the amount of charge on an ionized monomer, and $n_{ii}(\alpha,z)$ is a Kronecker delta function that equals one if there is a monomer of polymer ii at layer , and zero otherwise. In the same term, $\psi(z)$ is the electric potential at layer . In the last term of Equation 4, $f_{H^+}$is the fraction of charged monomers, which is given by (Equation 5):

$$\frac{f_{H^+}(z)}{\left(1-f_{H^+}(z)\right)}=\frac{\emptyset_{H^+}(z)}{K_a^{\circ}\,\emptyset_{\omega}(z)} \qquad (5)$$

The number of probabilities that are needed to describe the system should increase as the set of ligand-receptor binding increases in this model. This shows that the probability of having a spacer, ligand or bound ligand complex at specific configuration is only affected by the steric, van der Waals, and electrostatic interactions.

The volume fraction profile of all molecular species in the system is given by the following Relations (Equation 6):

$$\begin{aligned}
&\emptyset_{\omega}(z)=\exp\left(-\beta\pi(z)\upsilon_{\omega}\right)\\
&\emptyset_{H^+}(z)=\exp\left(-\beta\mu^{\circ}_{H^+}-\beta\pi(z)\upsilon_{\omega}-\beta q_{H^+}\psi(z)\right)\\
&\emptyset_{OH^-}(z)=\exp\left(-\beta\mu^{\circ}_{OH^-}-\beta\pi(z)\upsilon_{\omega}-\beta q_{OH^-}\psi(z)\right) \qquad (6)\\
&\emptyset_{+}(z)=\exp\left(\beta_{\mu+}-\beta\pi(z)\upsilon_{\omega}-\beta q_{+}\psi(z)\right)\\
&\emptyset_{-}(z)=\exp\left(\beta_{\mu-}-\beta\pi(z)\upsilon_{\omega}-\beta q_{-}\psi(z)\right)
\end{aligned}$$

where, , and are the standard chemical potential, and the amount of charge for specie *jj* respectively. In this system, we assume that all molecules have the volume of the solvent molecule (water molecule).

The general equation for the fraction of set of ligand-receptor binding is given by the following relation (Equation 7):

$$\frac{f_{LR_i}}{\left(1-\sum_{i=1}^{2}f_{LR_i}\right)}=\frac{C\,K_{LR_i}\,q_{LR_i}{}^{e}}{q_L\,\emptyset_{R_i}}\left(1-\frac{\sigma_p{}^{X_L}f_{LR_i}}{\sigma_{R_i}}\right) \qquad (7)$$

The maximum fraction of binding for these inputs and according to Equation 7 is $f_{LR1}=f_{LR2}=0.08$, and we choose it to be equal to 0.07.

where, is the partition function for free ligand complexes and q_{LR_i} is the partition function for the set i of bound ligand complexes. C constant comes from the association constant equation $K_{LR_i}=C\exp\left(-\beta\left(\mu^{\circ}_{LR_i}-\mu^{\circ}_{L}-\mu^{\circ}_{R_i}\right)\right)$, $\emptyset_{R_i}$ is the volume fraction of receptors on the interacting cell surface at a specific microstate, which can be calculated by knowing the receptors density and the cell-surface interaction area, and e is the base of the natural logarithm.The system is solved numerically by discretizing the system into number of layers with thickness of 0.33 nm. This complex non-linear system is composed of nine sets of unknowns. There are four unknown average volume fractions: for spacers, complex ligands, and two sets of bound complex ligands $\left(\langle\emptyset_s(z)\rangle,\langle\emptyset_L(z)\rangle,\langle\emptyset_{LR_1}(z)\rangle,\langle\emptyset_{LR_2}(z)\rangle\right)$. Another four unknowns are the fraction of inter-molecular interactions: for spacers, complex ligands, and two sets of bound complex ligands $\left(\langle\eta_s(z)\rangle,\langle\eta_L(z)\rangle,\langle\eta_{LR_1}(z)\rangle,\langle\eta_{LR_2}(z)\rangle\right)$. he electric potential pro ile $(\psi(z))$is the last unknown. We use the minimized free energy Equations 3 to 6, and Poisson equation to solve for the nine sets of unknowns. Exterminimizing the free energy with respect to the electric potential gives Poisson equation in the following form (Equation 8): $\frac{d^2\psi(z)}{dz^2}=-\frac{\langle\rho_q(z)\rangle}{\epsilon}$ (8)Where is the permittivity constant of the medium, which we assume to be water

$\langle\rho_q(z)\rangle=f_{H^+}(z)q_p\left(\langle\rho_L(z)\rangle+\langle\rho_{LR_1}(z)\rangle+\langle\rho_{LR_2}(z)\rangle\right)$

$+\sum_m q_m\,\rho_m(z)$, is the charge

density of all molecules in the system, where is the amount of charge on a charged polymer segment, while $q_{jj}$is the amount of charge on a specie jj that has a density of $\rho_{jj}(z)$ at layer . The electric potential profile is subject to two boundaries: the charge density on the cell surface $\sigma_{q_{cell}}$ and the charges on the micellar surface $\sigma_{q_{micelle}}$ which depends on the number of charged polymer segments that are attached to that surface (Equation9).

$$\frac{\partial\psi(z)}{z}\Big|_{z=1}=\frac{-\sigma_{q_{micelle}}}{\epsilon}\Rightarrow\frac{\psi(2)-\psi(1)}{\Delta}=\frac{-\sigma_{q_{micelle}}}{\epsilon}$$

$$(9)\ \frac{\partial\psi(z)}{\partial z}\Big|_{z=L}=\frac{-\sigma_{q_{cell}}}{\epsilon}\Rightarrow\frac{\psi(L-1)-\psi(L)}{\Delta}=\frac{-\sigma_{q_{cell}}}{\epsilon}$$

Where, =1 and =L are our boundaries, and =2 and z=$L-1$ are the first layers encountered as we move toward the middle of the system.

We solve Poisson equation by calculating the number of charged monomers on both the micellar surface and the cell surface if there are any. The cell surface has additional charge due to the density of charge on the cell. The system is solved twice. Firstly, to find the number of monomers on the cell, and secondly to use these inputs to solve for Poisson equation.

Results and Discussion

The system is modeled in a cubic lattice structure and discretized into discrete layers in the *XY* plane. he thickness of the layers is set to be equal to 0.33 nm for all calculations. he system contains four different kinds of polymer chains each consisting of 25 monomers. The salt concentration is maintained at 0.1 *molar* during all calculations. As mentioned in the previous section, this system composed of nine sets of unknowns. The nonlinear system is solved using KINSOL solver from the SUNDIALS library with SPGMR interface.

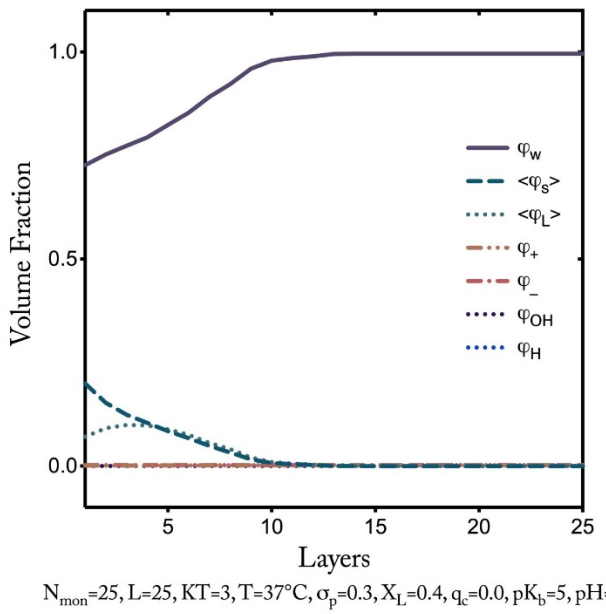

Figure 4: An illustration of the incompressibility constraint.

The system's solution is tested first by plotting the incompressibility constraint, and Figure 4 illustrates the validation of the constraint. The plot shows that the sum of the volume fraction of all molecules in the system at each layer goes to one. Notice that at a distance from the cell, the average volume fraction of all free ions in the system $\left(\emptyset_+,\ \emptyset_-,\ \emptyset_{H^+},\ \emptyset_{OH^-}\right)$ approaches zero. The incompressibility is tested at the following dependent variables values: the polymer density $\left(\sigma_p = \frac{0.3}{nm^2}\right)$, the separation distance between the cell surface and the micellar surface (L=25), the fraction of ligand complexes (X_L=0.4), their pKa=6, K_BT=3.0, the local temperature ($T = 37$ ℃) and the local pH=7.Because of the complexity of the system and the large number of unknowns, we also tested the solver by looking at the electric potential profile. Here we tested the system with previous inputs in two cases. The first case is when the micelle is at a distance from the charged cell surface $\left(\sigma_{q_{cell}} = \ -0.12,\ \ and + 0.12\right)$ at which we expect the electric potential to reach a zero domain between the two charged surfaces (the micellar surface is charged due to the charged grafted monomers on its surface). The second case is when the charged cell surface is close to the micellar surface (L=10) at which we don't see the zero domain in the middle of the system. Figure 5 shows the validation of the expected behavior for the electric potential profile.

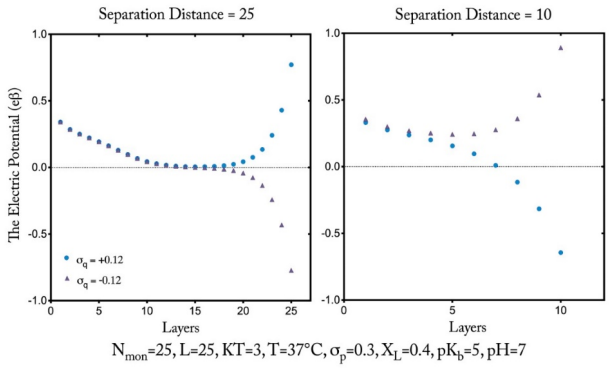

Figure 5: The effect of the distance between the micellar surface and the cell surface on the electric potential profile.

The dual-ligand technique is expected to improve the binding efficiency and selectivity. Here we will compare the number of bound ligands in the case of two different mono-ligands and a dual-ligand. In Figure 6, we see the average volume fraction of: bound receptors to mono ligand (L_1), bound receptors to mono-ligand (L_2), total bound receptors to both mono-ligands (L_1 + L_2), and those bound to dual-ligand (L_{12}) at two different pKa values (3 and 5). he dependent variables for these results are chosen to be as follow: $\left(\sigma_p = \frac{0.3}{nm^2},\ X_L = 0.4, L = 8,\ \sigma_q = \ -0.06,\ pH = 5.5,\ K_BT = 3.5,.\right.$ $\left.T = 39\ ℃\right)$

These parameters are chosen carefully depending on the cancer cell properties and the system behavior that we learned from our previous mono-ligand micelle model [28]. According to Equation 7 there is a precise range of the fraction of ligand-receptor binding for different choices of polymer density and fraction of ligands at which the $\left(1 - \frac{\sigma_p X_L f_{LR_i}}{\sigma_{R_i}}\right)$ value has to be positive. For this system, and with receptors density reaching up to 0.01, the maximum fraction of bound receptors is 0.08.

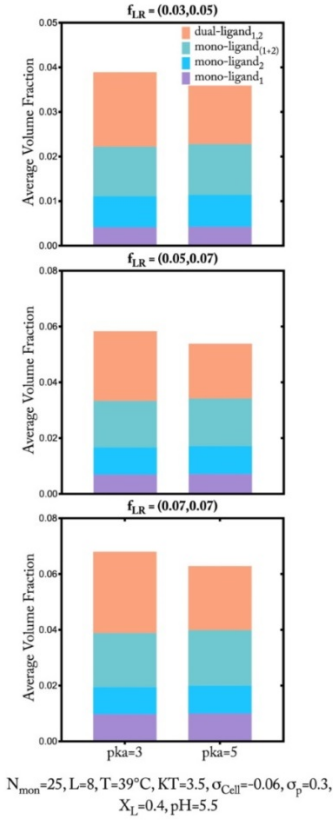

Figure 6: The efficiency of the dual-ligand technique and the effect of the pK_a values on the average volume fraction of binding.

Figure 6 has three diagrams each representing two different fractions of binding for two pK_a groups. In the first diagram, and for each group: the first column is the average volume fraction of a mono-ligand with f_{LR}=0.03, the second is the average volume fraction of a mono-ligand with f_{LR}=0.05, the third column is the sum of the average volume fractions of the two previous columns, and the last is the average volume fraction of dual-bound ligand that has a fraction of binding of 0.03 to the first targeted receptor and 0.05 to the second targeted receptor. The same is applied to the other two diagrams with different fraction of binding values.

Notice that the average volume fraction of a dual-ligand always exceeds the sum of the average volume fraction values of two mono-ligands that have the same fractions of binding as the dual-ligand. Since the dual-ligand has the affinity to bind to two receptors on the cell surface, its chance of binding should be higher than a mono-ligand that has an affinity to only one receptor on the cell surface. Thus, the dual-ligand technique seems to improve the binding efficiency.

Figure 6 also shows that the binding efficiency depends on the polyelectrolyte pK_a value. We see more binding at pK_a=3 than at pK_a=5. Moreover, increasing the pK_a value to 6 causes no ligand-receptor binding in both the mono-ligand system and the dual-ligand system. At pK_a=6 the average volume fraction of monomers decreases dramatically away from the micellar surface as the polyelectrolytes collapse.

$$pK_a \downarrow \rightarrow H^+ \uparrow \Rightarrow BH^+ \uparrow \Rightarrow \text{Stretched chains}$$

$$pK_a \uparrow \rightarrow H^+ \downarrow \Rightarrow BH^+ \downarrow \Rightarrow \text{Collapsed chains}$$

To study the dual-ligand design selectivity, we set the micelle dependent variables at:

$\left(\sigma_q = \frac{0.3}{nm^2},\ X_L = 0.4,\ L = 8,\ pK_a = 3{:}6\right)$.For each pK_a value we calculated the average volume fraction of bound dual-ligands for three different cases: cancerous cell with dependent variables $\left(\sigma_q = -0.06,\ pH = 5.5,\ K_BT = 3.5,\ T = 39\ ℃\ ,\ \sigma_{R1} = \sigma_{R2} = 0.01\right)$ healthy cell with the same density of receptors as the cancer cell $\left(\sigma_q = -0.02,\quad pH = 7,\quad K_BT = 3.0,\quad T = 37\ ℃\ ,\quad \sigma_{R1} = \sigma_{R2} = 0.01\right)$ and healthy cell with 10% lower receptor density than the cancer cell $\left(\sigma_q = -0.02,\quad pH = 7,\quad K_BT = 3.0,\quad T = 37\ ℃\ ,\quad \sigma_{R1} = \sigma_{R2} = 0.001\right)$

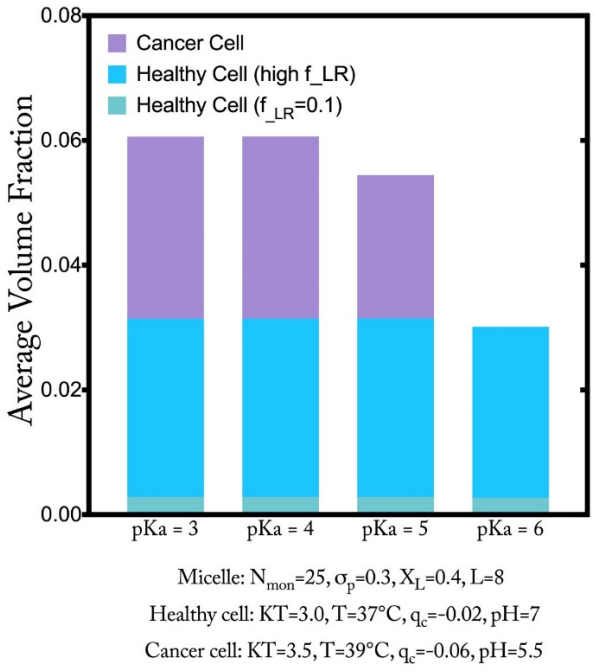

Figure 7: The diagram shows that the dual-ligand selectivity depends on the density of receptors on the surface of the cell.

Figure 7 shows that at low pK_a values (pK_a=3, 4), changing the local environment from a cancerous to a healthy cell environment decreases the average volume fraction of bound dual-ligands slightly if the number of receptors on both cells are the same.

However, at pK_a=5 the average volume fraction of bound dual-ligands increases at healthy cell environment. At pK_a values higher than 6, we see no binding to receptors on cancer cells, while dual-ligands bind to a good number of receptors on healthy cells. The base-

polyelectrolytes collapse at high pH values prohibiting the dual-ligands from reaching the cell surface.

At cancer cell: $pH \downarrow \rightarrow H^+ \downarrow \Rightarrow BH^+ \downarrow \Rightarrow$ Collapsed chains

At healthy cell: $pH \uparrow \rightarrow H^+ \uparrow \Rightarrow BH^+ \uparrow \Rightarrow$ Stretched chains

In the case of healthy cells with 10% less receptors on their surface than cancer cells, the average volume fraction of bound dual-ligands deceases dramatically. Meaning that the dual-ligand is near the cell surface as it stretches in the healthy cell environment. If a targeted receptor presented on the healthy cell surface, there could be a high probability that a dual-ligand to bind to that receptor. Thus, the dual-ligand technique doesn't seem to improve the selectivity above the mono-ligand technique. The selectivity can be improved if the stability of the micelle on the cell requires more than one dual-ligand to bind to the cell. The binding to one receptor on the cell shouldn't be enough to stabilize the micelle against the blood stream. In a previous work, we mentioned the importance of the size of the therapeutic micelle in improving the selectivity. We calculated the size of the therapeutic micelle depending on the density of receptors of the targeted cell. Using the dual-ligand technique with a micelle that has the right therapeutic size should improve both the selectivity and the efficiency.

Conclusion

We generalize a molecular theory that accounts for steric, van der Waals, and electrostatic interactions in a biological system to study the dual-ligand binding protocols. We used a decoupled mean-field approach to improve the van der Waals inter-molecular interaction efficiency. Different stimuli in the system affected the dual-ligand binding; however we found that the system local pH and the polyelectrolytes pK_a values are the driving parameters in the system. This could be highly related to the way the polyelectrolytes get ionized in the system. In our system we choose polyelectrolytes that bind to hydrogen ions to become positively charged. The system behavior could change in the case of polybases that dissociate to hydroxide groups and positively charged ions, which we may consider as a future work. We found that the dual-ligand technique should improve the binding efficiency and selectivity to cancer cells that have over-expressed receptors. The technique can be further improved by using the optimum therapeutic micellar size.

References

1. Sun H, Y Dong, J Feijen, Z Zhong (2018) Peptide-decorated polymeric nanomedicines for precision cancer therapy. J Control Release 290:11 – 27.
2. Teijeiro-Valino C, R Novoa-Carballal, E Borrajo, A Vidal, M Alonso-Nocelo, et al. (2018) A multifunctional drug nanocarrier for efficient anticancer therapy. J Control Release294: 154-164.
3. Yu X, I Trase, M Ren, K Duval, X Guo (2016) Design of nanoparticle based carriers for targeted drug delivery. Journal of Nanomaterials 2016:1–15.
4. Kedar U, P Phutane, S Shidhaye, V Kadam (2010) Advances in polymeric micelles for drug delivery and tumor targeting. Nanomedicine 6:714–729.
5. Deng C, Y Jiang, R Cheng, F Meng, Z Zhong (2012) Biodegradable polymeric micelles for targeted and controlled anticancer drug delivery: Promises, progress and prospects. Nano Today 7:467–480.
6. Abu Lila AS, T Ishida, H Kiwada (2010) Targeting anticancer drugs to tumor vasculature using cationic liposomes. Pharmaceutical Research 27:1171–1183.
7. Yang F, C Jin, Y Jiang, J Li, Y Di (2011) Liposome based delivery systems in pancreatic cancer treatment: From bench to bedside. Cancer Treatment Reviews 37:633–642.
8. Zhu D, S Wu, C Hu, Z Chen, Y Qin (2017) Doxorubicinloaded 'flower-like' polymeric nanoparticles for cancer therapy. J Control Release 259:e27–e28.
9. Barreto JA, WO Malley, M Kubeil, B Graham, H Stephan, L Spiccia (2011) Nanomaterials: Applications in cancer imaging and therapy. Adv Mater 23:H18–H40.
10. Noble GT, JF Stefanick, JD Ashley, T Kiziltepe, B. Bilgicer (2014) Ligand-targeted liposome design: Challenges and fundamental considerations. Trends in Biotechnology 32:32–45.
11. Egusquiaguirre SP, M Igartua, RM Hern andez, JL Pedraz (2012) Nanoparticle delivery systems for cancer therapy: Advances in clinical and preclinical research. Clin Transl Oncol 14:83–93.
12. Petros R A, JM DeSimone (2010) Strategies in the design of nanoparticles for therapeutic applications. Nat Rev Drug Discov 9:615–627.
13. Wang AZ, R Langer, OC Farokhzad (2012) Nanoparticle delivery of cancer drugs. Annu Rev Med 63:185.
14. Xiong L, X Du, F Kleitz, SZ Qiao (2015) Cancer-cell-specific nuclear-targeted drug delivery by dual-ligand-modified mesoporous silica nanoparticles. Small 11:5919 – 5926.
15. Mitchell RA, RB Luwor, AW Burgess (2018) Epidermal growth factor receptor: Structure-function informing the design of anticancer therapeutics. Exp Cell Res 371:1 – 19.
16. Brannon-Peppas L, JO Blanchette (2012) Nanoparticle and targeted systems for cancer therapy. Adv Drug Deliv Rev 64:206 – 212.
17. Quintana A, E Raczka, L Piehler, I Lee, A Myc, el at. (2002) Design and function of a dendrimer-based therapeutic nanodevice targeted to tumor cells through the folate receptor. Pharm Res 19:1310–1316.
18. Lu Y, PS Low (2003) Immunotherapy of folate receptor-expressing tumors: Review of recent advances and future prospects. J Control Release 91:17 –29.
19. Martinelli E, R De Palma, M Orditura, F De Vita, F Ciardiello (2009) Antiepidermal growth factor receptor monoclonal antibodies in cancer therapy. Clin Exp Immunol 158:1–9.
20. Sandoval MA, BR Sloat, DS Lansakara P, A Kumar, BL Rodriguez, et at. (2011) EGFR-targeted stearoyl gemcitabine nanoparticles show enhanced anti-tumor activity. J Control Release 157:287 – 296.
21. Yoo HS, TG Park (2004) Folate receptor targeted biodegradable polymeric doxorubicin micelles. J Control Release 96:273 – 283.
22. Sandoval MA, BR. Sloat, DS Lansakara-P, A Kumar, BL Rodriguez,et at. (2011) EGFR-targeted stearoyl gemcitabine nanoparticles show enhanced anti-tumor activity. J Control Release 157:287 – 296.
23. Aldaais EA (2016) A Theoretical Study of Polymer Based Drug Delivery Systems. Ph.D. Thesis, University of South Carolina.
24. Aldaais EA (2018) Generalized Theory of Monoligand-Receptor Binding for the Improvement of Nanoparticle Design. J Nanomed Nanotechnol 9:512.
25. Saul JM, AV Annapragada, RV Bellamkonda (2006) A dual-ligand approach for enhancing targeting selectivity of therapeutic nanocarriers. Journal of Controlled Release 114:277–287.
26. Takara K, H Hatakeyama, G Kibria, N Ohga, K Hida, H Harashima (2012) Size-controlled, dual-ligand modified liposomes that target the tumor vasculature show promise for use in drug-resistant cancer therapy. J Control Release 162:225–232.
27. Li X, H Zhou, L Yang, G Du, AS Pai-Panandiker, X Huang, B Yan (2011) Enhancement of cell recognition in vitro by dual-ligand cancer targeting gold nanoparticles. Biomaterials 32:2540–2545.
28. Yu J, X Xie, X Xu, L Zhang, X Zhou, et al. (2014) Development of dual ligand-targeted polymeric micelles as drug carriers for cancer therapy in vitro and in vivo. Journal of Materials Chemistry B 2:2114–13.
29. Gao Y, C Zhang, Y Zhou, J Li, L Zhao, et al. (2015) Endosomal pH-Responsive polymer-based dual-ligand-modified micellar nanoparticles

for tumor Targeted delivery and facilitated intracellular release of paclitaxel. Pharm Res 32:1–14.

30. Chen H, F Chen, Y Chen, Y Zeng, X Qi, et al. (2018) Targeted salinomycin delivery with EGFR and CD133 aptamers based dual-ligand lipid-polymer nanoparticles to both osteosarcoma cells and cancer stem cells. Nanomedicine 14:2115–2127.
31. Wan Y, Y Liu, PB Allen, W Asghar, MAI Mahmood, et al. (2012) Capture, isolation and release of cancer cells with aptamer-functionalized glass bead array. Lab on a Chip 12:4693–10.
32. Ma H, J Liu, MM Ali, MAI Mahmood, L Labanieh, M Lu, et al. (2015) Nucleic acid aptamers in cancer research, diagnosis and therapy. Chem Soc Rev 1–17.
33. Noh T, YH Kook, C Park, H Youn, H Kim, et al. (2008) Block copolymer micelles conjugated with anti-EGFR antibody for targeted delivery of anticancer drug. Journal of Polymer Science Part A: Polymer Chemistry 46:7321–7331.
34. Zhang F, S Wang L Yin Y Yang, Y Guan, W Wang, et al. (2015) Quantification of epidermal growth factor receptor expression level and binding kinetics on cell surfaces by surface plasmon resonance imaging. Anal Chem 87:9960–9965.
35. Sandoval MA, BR Sloat, DSP Lansakara P, A Kumar, BL Rodriguez, et al. (2012) EGFR-targeted stearoyl gemcitabine nanoparticles show enhanced anti-tumor activity. J Control Release 157:287–296.
36. Rosenbluth MN, AW Rosenbluth (1955) Monte carlo calculation of the average extension of molecular chains. The Journal of Chemical Physics 23:356–5.
37. Aldaais EA (2019) New method of increased accuracy for the calculation of intermolecular interactions in thermotropic polymers. Results in Materials 1:100013.